




Elastic and phonon-mode anomalies with temperature in the energetic material $C_6H_6N_4O_8$ Soumee Chakraborty ^{1,*}, R. Rajitha ¹, V. Venkatesan,² Anuj A. Vargeese,³ R. Raja Madhavan,⁴
R. Asuvathraman,⁴ and T. R. Ravindran ¹¹*Materials Science Group, Homi Bhabha National Institute (HBNI), Indira Gandhi Centre for Atomic Research, Kalpakkam 603102, Tamil Nadu, India*²*Research & Innovation Centre, IIT Madras Research Park, Chennai 600113, Tamil Nadu, India*³*Department of Chemistry, National Institute of Technology Calicut, Calicut 673601, Kerala, India*⁴*Materials Chemistry & Metal Fuel Cycle Group, Indira Gandhi Centre for Atomic Research, Kalpakkam 603102, Tamil Nadu, India*

(Received 15 November 2021; revised 2 March 2022; accepted 29 March 2022; published 12 April 2022)

Temperature-dependent Brillouin and Raman spectroscopic investigations are carried out on energetic material 4,10-Dinitro-2,6,8,12-tetraoxa-4,10-diazatetracyclo [5.5.0.0^{5,9}.0^{3,11}] -dodecane (TEX; $C_6H_6N_4O_8$) from -196 to 180 °C, close to its sublimation point, to study its elastic and phonon mode behaviors. Ambient values of experimental shear (G) and bulk (K) moduli of TEX are obtained as $G = 5.6$ GPa and $K = 17.7$ GPa. We have computed the elastic tensor and obtained the averaged bulk and shear moduli to compare with the experimentally obtained polycrystalline values. The known lower sensitivity of TEX compared with similar caged secondary explosives as CL-20, Royal Demolition eXplosive, and β -High Melting eXplosive is reckoned as due to its inherently high bulk modulus. We report direct experimental evidence of rapid reduction in elastic constant of TEX from 20 to 80 °C, much before its melting point. Though there are no phase transitions in this temperature span, all Raman bands exhibit softening behavior around this temperature. We observe two distinct anomalies. Some bending modes such as bending of CNC (356 cm^{-1}), in-plane bending of NNO (552 cm^{-1}), bending of NCO (610 cm^{-1}), in-plane bending of NNO (635 cm^{-1}), and in-plane bending of ONO and OCO (712 cm^{-1}) exhibit slight hardening before and after the elastic anomaly. However, the asymmetric stretching modes at 1574 cm^{-1} (asymmetric stretch of NO) and 1590 cm^{-1} (asymmetric stretch of NO_2) exhibit hardening below 20 °C but soften after 80 °C. This hardening switching over to softening above the anomaly indicates a release of stiffness manifesting from a conformational change to exo-endo and aiding the increasing compressibility. Emergence of new diffraction peaks ~ 50 °C and even observed at 150 °C, which is well above the elastic anomaly, suggests that the material at high temperature may be isostructural to that at low temperature. In this paper, we establish that the high bulk modulus value of TEX contributes to its lower sensitivity; however, we also clearly demonstrate reduction in elastic modulus accompanied by anomalous behavior of Raman modes. This decrease in elastic modulus leading to increased compressibility may result in increased sensitivity of the explosive material just above room temperature.

DOI: [10.1103/PhysRevB.105.134105](https://doi.org/10.1103/PhysRevB.105.134105)**I. INTRODUCTION**

Explosives are energetic materials that are widely used in both civilian and military domains. The performance of an explosive critically depends on its density, energy of decomposition reaction, rate of energy release (velocity of propagation wave), and molecular weight of the gaseous products [1]. Furthermore, an increase in oxygen balance and heat of formation generally increases both sensitivity and performance [1]. In this context, sensitivity refers to vulnerability to unintended and undesired detonation initiated by an accidental stimulus such as heat, friction, spark, impact, and shock [2,3]. Special care must be taken during handling of these compounds. They must not easily undergo decomposition in the presence of heat, mechanical shock, or exposure to certain

chemical reagents. Therefore, an ideal explosive is one which has high performance but is insensitive enough to be handled safely during its use, storage, and transport [3]. Improved thermal stability of energetic materials ensures safer production, increased shelf life of munitions, and low vulnerability to accidental initiations. Therefore, some favorable attributes for such explosives include high thermal stability, chemical stability, favorable oxygen balance, and high density to attain high performance with low sensitivity [1].

Primary explosives are more sensitive to external stimuli, while secondary explosives need a strong stimulus from a primary explosive to detonate [4]. The sensitivity of any explosive can be related to the chemical nature of the material and is highly dependent on the molecular arrangements and intermolecular or lattice interactions [2]. There are numerous correlations that have been proposed between impact sensitivity and molecular/crystalline properties such as bond energies, bond lengths, bond polarities, electrostatic potentials, nuclear magnetic resonance chemical shifts, rates of

*Corresponding author:
soumee.chakraborty@gmail.com, soumee@igcar.gov.in

vibrational energy transfer, heats of fusion, etc. [3]. Moreover, impact sensitivities are also dependent on quality, size, shape, purity, lattice defects, surface roughness, and granulometry of crystals [3]. Despite this, there is no single equation to relate sensitivity to performance and molecular structure of any individual energetic material [2].

Knowledge of material structure and solid deformation mechanics is fundamental to predict explosive behavior in precision applications. Since secondary explosives are molecular solids made of organic molecules, they are highly compressible and typically undergo polymorphic phase transitions [4]. The compressibility of explosive material is an important factor in predicting the peak pressure achieved upon detonation. A key aspect of explosive performance and safety relates to the translation of thermomechanical stimuli to the chemical energy response. Even though it remains a difficult task to link mechanisms [5] directly to initiation pathways, it has been established theoretically and experimentally that material perturbations lead to energy localizations, resulting in hotspot formation and onset of chemical reactions [6]. The impact and shock sensitivities of energetic materials with similar molecular structure also depend on the ease of energy transfer [7] from the skeletal vibrations of the lattice to the high-frequency atomic vibrations with spontaneous localization of vibrational energy in the explosophore groups of the molecules leading to detonation [2]. Therefore, structural and elastic deformation studies under various stimuli are required to be undertaken for safety analysis [8].

One of the approaches used to synthesize insensitive high explosives is to incorporate maximum possible percentage of nitrogen into energetic materials [1]. Materials of the heterocyclic strained ring-and-cage families (heteroaromatic nitro compounds) represent a class of secondary explosives capable of delivering higher performance, reduced sensitivity to external shock, and other stimuli compared with analogous aromatic systems. Among these polycyclic compounds, 4,10-Dinitro-2,6,8,12-tetraoxa-4,10-diazatetracyclo[5.5.0.0^{5,9}.0^{3,11}]-dodecane (TEX) [9,10] is a candidate material for high-performance insensitive explosives [10,11] characterized by a high density (1.985 g/cc), excellent thermal stability (sublimation >240 °C) [12,13], and velocity of detonation (8665 m/s). TEX is a caged polynitramine [14,15] and is much less sensitive to friction (>353 N) and impact (23 J) stimuli [16] than other high-performance explosives, such as Royal Demolition eXplosive (RDX) and High Melting eXplosive (HMX). There are correlations reported between elastic constants and ease of detonation initiation in such secondary explosives [17]. These reports have demonstrated both experimentally [17,18] and theoretically [19,20] the complete set of elastic tensor for crystalline explosives [20]. Even though a lot of work has been reported [21] on the chemical, physical, detonation [22], and explosive properties of TEX [23], studies concerning its elastic constants and their significance to its insensitivity are lacking. Furthermore, there are no studies of temperature dependence of elastic properties of insensitive high explosive materials which potentially affect their sensitivity under thermal agitation. Any variation in elastic properties with temperature and/or pressure will alter the performance of the explosive, and therefore, such structural investigations are

to be pursued systematically. In this paper, we present the elastic constants of polycrystalline TEX and investigate the temperature dependence of the Brillouin and Raman modes of TEX which directly correlate to the elastic and bonding properties of the crystal. The aims of this paper are (i) to obtain the elastic constants of TEX, (ii) to investigate the behavior of its acoustic and optical phonon modes as a function of temperature, (iii) to look for any anomalous changes in the mode frequency and elastic behavior, and (iv) to ascertain the structural stability until the material approaches its melting point (m.p.). We also report direct experimental evidence of a sudden reduction in elastic constants of TEX much before its m.p.

II. EXPERIMENTAL

TEX was synthesized in a two-step process. First, 10 mL aqueous NaOH solution was slowly added to 100 g of aqueous glyoxal solution and cooled to 10 °C. Then 31 mg of formamide was added dropwise to this mixture, and thereafter, the temperature of the reaction mixture was increased to 25 °C. This temperature was maintained until a solid product precipitated. The filtered solid was then washed with water and acetone and dried overnight. A white solid of 1,4-dimethyl-2,3,5,6-tetrahydroxypiperazine (THDFP) was obtained. In the second step, glyoxal was added to a solution of sulfuric acid at 0 °C. To this, the earlier-prepared THDFP was added slowly. This mixture was stirred for 5 h, after which the temperature was reduced to -5 °C. Fuming nitric acid was added slowly to this mixture, which was continuously stirred at room temperature for 48 h and then poured onto crushed ice. The solid product was filtered, washed with aqueous ethanol, and dried. This solid was then recrystallized from a 1:1 mixture of acetone and methanol solvents to obtain crystalline, pure TEX. The details of the synthesis can be found elsewhere [4].

Brillouin spectra were recorded in the backscattering geometry with a 3 + 3 pass tandem Fabry-Perot interferometer (JRS Instruments), using a 532 nm single longitudinal mode diode-pumped solid state laser. The spectra were recorded between -196 and 180 °C using a LINKAM heating/cooling stage. Mode frequencies and line widths were obtained by least squares fitting of the spectra to a set of Lorentzian profiles using PEAKFIT software.

Raman spectra were excited by the 514.5 nm line of an Ar⁺ laser and recorded in the backscattering geometry using a micro-Raman spectrometer (Renishaw model InVia). The TEX sample was placed inside the heating/cooling stage for temperature-dependent studies from -196 to 180 °C. The Raman spectra were analyzed to obtain mode frequencies using Lorentzian peak fitting.

X-ray diffraction (XRD) was carried out on TEX powder sample with Cu K α radiation using a PANalytical X'Pert Pro MPD x-ray diffractometer coupled with an Anton Paar HTK16 high-temperature attachment. The sample was mounted on a tantalum strip that was resistively heated, and the sample temperature was monitored with a thermocouple spot welded to the rear of the strip. All measurements were carried in a vacuum of $\sim 10^{-5}$ Torr. Diffractograms were recorded from 25 to 150 °C.

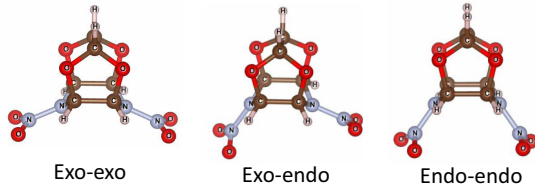


FIG. 1. The three different conformers of a TEX molecule (a rigid isowurtzitane cage comprising two five-membered rings and a six-membered ring): exo-exo, exo-endo, and endo-endo based on the orientation of the two nitro groups with respect to the six-membered ring. Adapted with permission [4].

The various conformers of TEX were obtained using the GAUSSIAN 09W program [24], with the B3LYP hybrid functional [25] and aug/cc-pVTZ basis set and the AVAGADRO software [26]. Elastic constants were calculated to compare the experimentally obtained values using the CASTEP code from Materials Studio Version 6.0 (Accelrys) package [27]. The electronic wave functions were obtained by using a density mixing minimization method for the self-consistent field calculation. Norm-conserving pseudopotentials and a plane-wave expansion of the wave functions are used. The Broyden, Fletcher, Goldfar, and Shannon (BFGS) method [28] was used for structure relaxation. The local density approximation functional proposed by Ceperley and Alder [29] and parametrized by Perdew and Zunger [30], named CA-PZ was employed. The calculations were performed by using an energy cutoff of 830 eV for a plane-wave basis set, and Brillouin zone sampling was performed by using the Monkhorst-Pack scheme [31] with k-point grid $1 \times 2 \times 1$. The experimental crystal structure of TEX was first relaxed to allow the ionic configuration, cell shape, and volume to change. The total energy of the system was converged to $<5.0 \times 10^{-6}$ eV, the residual force <0.01 eV/Å, the displacement of the atoms $<5 \times 10^{-4}$ Å, and the residual bulk stress <0.02 GPa during the geometry relaxation. This optimized structure is used for elastic constants calculation.

III. RESULTS AND DISCUSSION

The TEX molecule is a rigid isowurtzitane cage comprising two five-membered rings and a six-membered ring. It has three conformers: exo-exo, exo-endo, and endo-endo based on the orientation of the two nitro groups with respect to the six-membered cage, as depicted in Fig. 1. The exo-exo conformation is obtained by optimizing the TEX molecular structure using the GAUSSIAN 09W program, with the B3LYP hybrid functional and the aug/cc-pVTZ basis set [4]. While we tried to optimize exo-endo and endo-endo conformers of TEX using GAUSSIAN 09W, these structures converged to exo-exo conformation. Therefore, to obtain the exo-endo and endo-endo conformations, the dihedral angles corresponding to NO_2 orientation of the molecule about the ring (dihedral angles NNCC, ONNC) have been varied using the AVAGADRO software [4]. The structure with exo-exo conformers, termed as the α phase, is the most stable one reported using single-crystal XRD [14] and *ab initio* calculations [4]. TEX

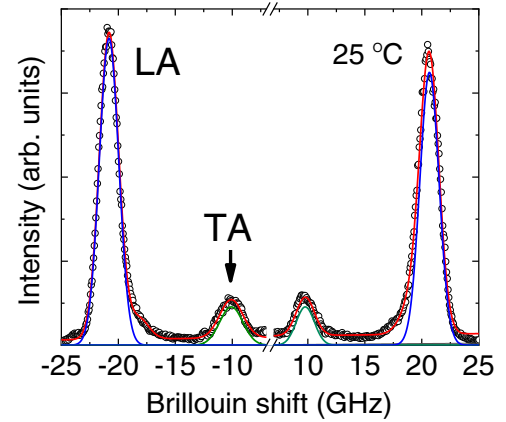


FIG. 2. Brillouin spectrum of TEX at 25 °C depicting the doublets of longitudinal acoustic (LA) and transverse acoustic (TA) modes. The experimental data are shown as open circles, while the fitted spectrum is given as a red continuous line. The blue curves exhibit the LA mode, while the green fitted peaks show the TA mode.

crystallizes in a triclinic structure (space group $P\bar{1}$) at ambient conditions.

The Brillouin spectrum of TEX (Fig. 2) exhibits peaks at 10 GHz [transverse acoustic (TA) mode] and 20.8 GHz [longitudinal acoustic (LA) mode] on the Stokes and anti-Stokes sides. However, for a triclinic structure, we expect one LA and two TA modes in the Brillouin spectrum. It can be noted that, in the present experiments, Brillouin scattering was measured from polycrystalline TEX. In elastically isotropic solids, such as a polycrystalline aggregate or a glass, the two transverse/shear modes have the same frequency. Only a pair of peaks appear on each side of the spectrum, and the elastic moduli are obtained directly from this single spectrum. Knowledge of mechanical behavior of polycrystalline solids is essential for engineering applications.

Brillouin scattering is inelastic scattering of light by acoustic phonons propagating through the lattice at the speed of sound. In the limiting value of phonon wave vector q , when visible light is the excitation source, the wavelengths of the acoustic phonons are approximately hundreds of unit cells. This allows the lattice to be modeled as an elastic continuum, and the acoustic phonon frequency (Brillouin shift) depends linearly on q , i.e., $\omega_B = Vq$, where V is the sound velocity. The dependence of the acoustic mode frequency on the scattering angle θ can be written as

$$\omega_B = 2Vn_0 \sin \frac{\theta}{2}, \quad (1)$$

where the incident photon wave vector $k_0 = n\omega_0/c$, n being the refractive index, $\omega_0 = 2\pi\nu_0$ is the angular frequency of the excitation laser, and c is the velocity of light in vacuum. Thus, sound velocity in the material can be determined directly from the Brillouin shift, and hence, elastic constants of the material can be calculated as

$$C = \rho V^2, \quad (2)$$

when the material density ρ is known. In the present experimental setup, θ is 180° for backscattering geometry. The refractive index of TEX at 532 nm (excitation wavelength

used in Brillouin spectroscopy) was estimated from computed reflectivity data [23] to be $n = 1.58$. Since the acoustic mode frequencies are a direct measure of the sound velocities governed by the elastic properties of the material, this refractive index was used to calculate the longitudinal (V_L) and transverse (V_T) sound velocities from the Brillouin shift (ν_B) using Eq. (1):

$$V = (\lambda \nu_B) / 2n, \quad (3)$$

where λ is the incident laser wavelength (532 nm) used. The spectrum in Fig. 2 was deconvoluted using multimode curve fitting to extract the frequency (ν_B) of the acoustic modes. The longitudinal and transverse sound velocities are respectively calculated to be 3567 and 1684 m/s using Eq. (3). The density of TEX is $\rho = 1.985$ g/cc, and the longitudinal and transverse elastic moduli are calculated as $C_L = 25.3$ GPa and $C_T = 5.6$ GPa, respectively. Being an elastically isotropic polycrystalline sample, the longitudinal (compressional) and transverse (shear) wave velocities are independent of the wave propagation direction, and they are related to the adiabatic bulk (K) and shear (G) moduli as

$$G = C_T, \quad (4)$$

$$K = C_L - \frac{4}{3}G. \quad (5)$$

Thus, the experimental shear (G) and bulk (K) moduli of TEX are obtained as $G = 5.6$ GPa and $K = 17.7$ GPa.

In addition, we computed the complete set of 21 independent components of the elastic tensor of triclinic TEX crystal from first-principles calculations based on density functional theory using Materials Studio (CASTEP). This is performed by relaxing the unit cell structure and then applying several small deformations. Thereafter, the resulting stress tensor is calculated, and the components of the elastic tensor are obtained as fitting parameters to the stress data. Optical properties such as refractive index were also calculated. The value of the refractive index at 532 nm was found to be 1.59. The obtained elastic tensor of a TEX crystal was checked for mechanical stability. It was found that the set of elastic components meet the Born stability criteria. The matrix is positive definite, and all eigenvalues are positive.

The longitudinal and shear sound speeds are direction independent in polycrystalline TEX (obtained using Brillouin scattering data) compared with the single crystal (computed using CASTEP) [32]. The relationship between single-crystal elastic components (represented by tensors, C_{ij}) and polycrystalline elastic constants (scalars, C_L and C_T) have been studied extensively in the literature using various averaging methods [33]. Tensor averages have been proposed for many physical properties such as elastic constants, dielectric constants, electrical and thermal conductivity, and piezoelectric constants [33]. Analysis of polycrystalline aggregates usually proceeds by assuming that the anisotropic crystals comprising them are randomly oriented in space, so the overall average elastic behavior can be well approximated by isotropic effective bulk and shear moduli using statistical homogenization techniques [34,35]. Among the various popular averaging methods, the Voigt and Reuss formulations assuming uniform strain and

uniform stress, respectively, form bounds in the homogenization techniques on the actual elastic properties [35]. Voigt [36] has shown that

$$9K_V = (C_{11} + C_{22} + C_{33}) + 2(C_{12} + C_{23} + C_{31}), \quad (6)$$

$$15G_V = (C_{11} + C_{22} + C_{33}) - (C_{12} + C_{23} + C_{31}) + 3(C_{44} + C_{55} + C_{66}), \quad (7)$$

while Reuss [36] has given

$$\frac{1}{K_R} = (S_{11} + S_{22} + S_{33}) + 2(S_{12} + S_{23} + S_{31}), \quad (8)$$

$$\frac{15}{G_R} = 4(S_{11} + S_{22} + S_{33}) - 4(S_{12} + S_{23} + S_{31}) + 3(S_{44} + S_{55} + S_{66}), \quad (9)$$

where K_V , G_V , K_R , and G_R are the Voigt bulk modulus, Voigt shear modulus, Reuss bulk modulus, and Reuss shear modulus, respectively, and C_{ij} and S_{ij} are the components of the elastic and compliance tensors. However, as seen in Eqs. (6)–(9), only 9 out of the 21 independent elastic constants of the single crystal appear in the Voigt and Reuss formalism for the macroscopic moduli. Furthermore, it is observed that the differences between the Voigt and Reuss bounds tend to be relatively large for compounds with small values of bulk and shear modulus. Hill [36] proposed improved estimates of the elastic constants by simply finding the arithmetic average of the Voigt and Reuss bounds:

$$K_H = \frac{K_V + K_R}{2}, \quad (10)$$

$$G_H = \frac{G_V + G_R}{2}. \quad (11)$$

The Hill estimate is commonly employed [37] because of its simplicity. The Hill estimates of the bulk and shear moduli of TEX are $K_H = 11.5$ GPa and $G_H = 8.9$ GPa, respectively. These computed values are not in good agreement with the experimentally arrived elastic constants. These discrepancies are attributed to the degree of elastic anisotropy and the underlying structure of TEX [35]. It has been further emphasized in the literature that good agreement between theory and experiment is expected only when the polycrystal approaches perfect disorder without texture or characteristic grain shapes [33]. It must be noted that discrepancies were reported [17] between theoretical studies and experimental work on indexed single crystals of a similar caged secondary explosive CL-20 [17]. However, CL-20 is very sensitive to friction (64 N), impact (4 J), and thermal stress resulting from steric strain of the nitramine groups [16]. Replacing four nitramine groups in CL-20 by ether bridges results in the molecular structure of TEX [16]. As TEX retains the isowurtzitan cage structure of CL-20, it conserves its high density; however, its sensitivity greatly reduces due to the absence of the four sterically demanding nitramine groups. It was argued that, even though potentials used in theoretical studies accurately reproduce static properties such as unit cell structure, they do not guarantee that the curvature of the potential surface would accurately predict dynamical properties such as vibrational frequencies or elastic properties of a given material [17]. This

TABLE I. Comparisons between the bulk (K) and shear (G) moduli obtained from Brillouin scattering studies on TEX and other popular secondary explosives. The values are in GPa.

Moduli (GPa)	TEX (Brillouin scattering on polycrystalline material: this paper)	TEX (CASTEP computed on single crystal: this paper)	ϵ -CL-20 (Brillouin scattering on single crystal) [17]	RDX (Brillouin scattering on single crystal) [7]	β -HMX (Brillouin scattering on single crystal) [17]
K_{Hill} or K	17.7	11.5	8.6	11.9	9.9
G_{Hill} or G	5.6	8.9	5.7	7.8	3.7

could explain why the foregoing theoretical values of elastic moduli do not match with our experimental data.

It is known from the literature that a stiffer lattice is less sensitive to detonation initiation from a hydrodynamic shock [17]. Table I lists the bulk and shear moduli of TEX and other similar secondary explosives ϵ -CL-20 (monoclinic), RDX (orthorhombic), and β -HMX [17]. TEX has the stiffest lattice among these popular secondary explosives, while the bulk modulus of RDX $>$ β -HMX $>$ ϵ -CL-20. It has been found that ϵ -CL-20 is more sensitive to shock-initiated detonation than HMX and RDX. Structurally, CL-20 is very much like TEX, as discussed earlier. The latter has been found to be much less sensitive than CL-20, probably due to its high elastic moduli, as seen here.

Apart from gaining information on the elastic stiffness constants, Brillouin spectroscopy is an efficient tool to probe the dynamical changes associated with density fluctuations in the structure of matter as a function of pressure or temperature [38]. The real part of the complex elastic modulus exhibits the ability of the structure to transmit elastic energy, while the imaginary component represents the viscous dissipation owing to structural disintegrity. This information is obtained from an analysis of temperature-dependent Brillouin spectra wherein the temperature dependence of the frequency of acoustic modes depicts the structural integrity, while the temperature dependence of width of the modes represents the damping of the elastic wave propagation.

From the Brillouin spectra of TEX at different temperatures [Fig. 3(a)], it can be observed that both LA and TA modes vary in frequency, reflecting changes in the elastic properties of the material with temperature. These spectra were fitted to obtain the LA and TA mode frequencies and widths. TA waves, as shown, are often less intense than LA waves. Moreover, TA modes have smaller energy shifts since the restoring forces associated with shear waves are weaker. This combination of lower intensities with smaller energy shifts in the vicinity of elastically scattered Rayleigh line results in masking of the TA modes. Although the positions of the TA modes are decipherable with fitting (see Fig. 2), the behavior of the TA modes are not discussed further. Figure 3(b) shows the temperature variation of the LA mode from the frequency and width extracted by fitting the Brillouin spectra at various temperatures. Initially, the mode frequency shows a slight inflation and then a gradually decreasing trend due to the usual increase of anharmonic effects with temperature. Thereafter, a sudden kink is observed at 20 °C, above which the LA mode frequency drops steeply. This reduction in frequency could indicate a disruption of the lattice for

structural relaxation and lattice reorientation. The monotonic steep slope continues until ~ 80 °C, after which the LA frequency stabilizes with a large scatter in the data. A narrow line width observed not too far below this transition [see Fig. 3(b)] implies a high degree of transmission of the elastic wave and much less energy dissipation by the propagating hypersound. However, in the same range of temperature from 20 to 80 °C, where the frequency exhibited an abrupt fall, the width of the LA mode exhibits almost no change and shows an increasing trend with a large scatter beyond this region. The absorption coefficient α_L for the LA mode, $\alpha_L = (\pi\Gamma)/V_L$, will show a similar dependence to the width (Γ). As described before, the imaginary part of the complex elastic modulus is reflected in the changes in the mode width. The increase in width of the LA mode indicates the damping of the longitudinal acoustic wave and hindrance to phonon propagation in the presence of structural imperfections. It can also signify broken and disordered molecules, leading to loss of network connectivity. These changes in the acoustic mode strongly suggest some changes in the conformation of the TEX molecules, changes in the bonding characteristics of the lattice, or even an order-disorder phase transition. However, our earlier high-temperature XRD results of TEX crystal confirm no structural transition in the temperature range of the present studies [39]. Moreover, thermogravimetric and differential scanning

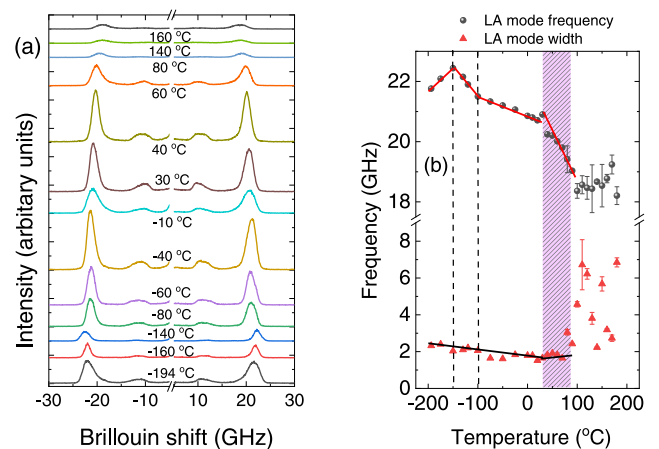


FIG. 3. (a) Brillouin spectra of TEX at selected temperatures. (b) Temperature variation of the longitudinal acoustic (LA) mode frequency (circles) and width (triangles). The lines through the data are guides to the eye. The shaded region depicts the temperature span of elastic anomaly.

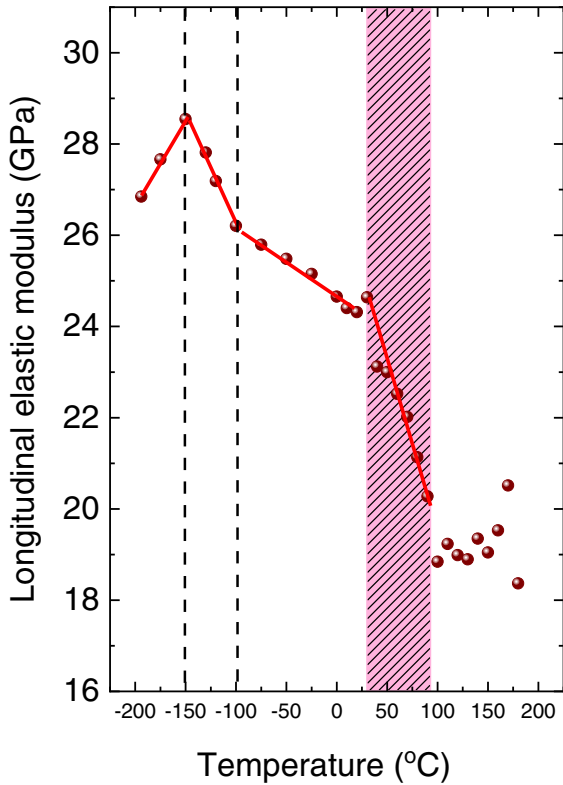


FIG. 4. Temperature dependence of longitudinal elastic modulus (C_L) of a TEX crystal depicting the kink at -150°C and the steep transition at 20°C . The shaded region marks the region of abrupt change. The lines through the data are guides to the eye.

calorimetric studies have demonstrated that TEX sublimes $\sim 240^\circ\text{C}$ [16] and decomposes $\sim 297^\circ\text{C}$ [12].

The temperature dependence of the refractive index of the TEX crystal is required to calculate the longitudinal sound velocities V_L using Eq. (3). Since the temperature dependence of density could be estimated from the lattice parameters obtained by fitting the experimentally measured XRD patterns of TEX [39], the temperature dependence of the refractive index was calculated using the Gladstone-Dale relation $n = \rho K + 1$ from the known values of density at those temperatures [40]. The constant K has been obtained using the room-temperature values of n and ρ . The sound velocities (V_L) thus obtained were used to calculate the temperature variation in longitudinal elastic modulus of TEX crystal using Eq. (2).

Figure 4 shows the temperature-dependent longitudinal elastic modulus (C_L) of the TEX crystal over a temperature span of $\sim 400^\circ\text{C}$. In this temperature span, the elastic constant varies from ~ 27 to 18 GPa. At lower temperatures, from -196 to $\sim 20^\circ\text{C}$, we observe a sudden kink $\sim -150^\circ\text{C}$ and then a gradual monotonic change. However, the longitudinal modulus exhibits a sudden drastic decrease of ~ 5 GPa across a small temperature range of 60°C from 20 to 80°C and thereafter does not change significantly. This region (depicted in Fig. 4 by the pink shaded part) indicates a relaxation or transition. The TEX crystal in this region becomes highly compressible, and the compressibility increases at a faster rate between 20 and 80°C . The rate of compressibility becomes almost constant thereafter until the material sublimates. This

may be due to a conformation change in the crystal. Our XRD results confirm the ambient phase as the α phase with exo-exo conformer [4]. Hence, the TEX molecules are in this conformation before the transition. The increase in compressibility refers to a decrease in stiffness in the transition range and may be due to the presence of mixed conformers resulting in decrease in cross-linking or reduction in intermolecular interactions, while the molecule may change to a different conformation $\sim 80^\circ\text{C}$. It must be noted that a change in conformation does not necessarily change the diffraction pattern, as we had observed in the pressure-dependent studies of TEX [4].

To gain more insight into the structural changes in TEX $\sim -150^\circ\text{C}$ and across the temperature range (20 – 80°C), where drastic softening of the longitudinal elastic modulus occurs, temperature-dependent Raman scattering investigations were carried out. As discussed above, at ambient conditions, TEX has a triclinic structure (space group $P\bar{1}$) with two molecular units per unit cell [39]. It has 24 atoms per molecule and therefore 144 acoustic and optical phonon modes. TEX being a molecular crystal, these phonons are classified into external (lattice) and internal (intramolecular) modes. Using factor group analysis, the following irreducible representation was obtained for TEX crystal: $\Gamma_{\text{total}}(144) = 72A_g + 72A_u = 6\Gamma_{\text{librations}} \{3A_g + 3A_u\} + 6\Gamma_{\text{lattice}} \{3A_g + 3A_u\} + 132\Gamma_{\text{internalmodes}} \{66A_g + 66A_u\}$. All A_g modes are Raman active. This implies there are 72 expected Raman modes. Figure 5(a) depicts the ambient Raman spectrum of TEX with 54 decipherable modes. The ordinate axis is shown in the log scale for unambiguous identification of the modes. The obtained number of modes is less than the expected number. It has to be noted that the low-frequency cutoff in this experiment is at 50 cm^{-1} . The libration mode at 44 cm^{-1} identified using CASTEP is not encompassed here. Moreover, a few other Raman active modes may be of too low intensity and hence may be below the detection limit of the present measurements. Figure 5(b) depicts the temperature-dependent Raman spectra of TEX at selected temperatures. At a first glance, the spectra look similar with no effect of temperature. There seems to be no appearance/disappearance of modes or any drastic change in relative intensities of the modes. However, modes which could be clearly traced as a function of temperature throughout the temperature range are considered for further analysis. Table II presents the normal mode assignments of the Raman-active modes which are analyzed for their temperature dependence. These modes are assigned [4] by visual examination of the vibrations using the Materials Studio package. They include lattice modes, librations, bending, torsion, and stretching of the various atoms and moieties in the unit cell. Most of the modes considered are strong in intensity; a few weak modes and shoulders are also analyzed.

Figures 6(a)–6(f) depict the temperature dependence of the mode frequencies presented in Table II. Most of the modes exhibit a clear monotonic softening at lower temperatures because of regular anharmonicity. However, a sudden and slight jump is observed at 20°C , above which the frequency exhibits a steep softening. Above $\sim 80^\circ\text{C}$, the frequency slope reduces again. This behavior is like what was observed for the elastic modulus through the temperature dependence of the acoustic

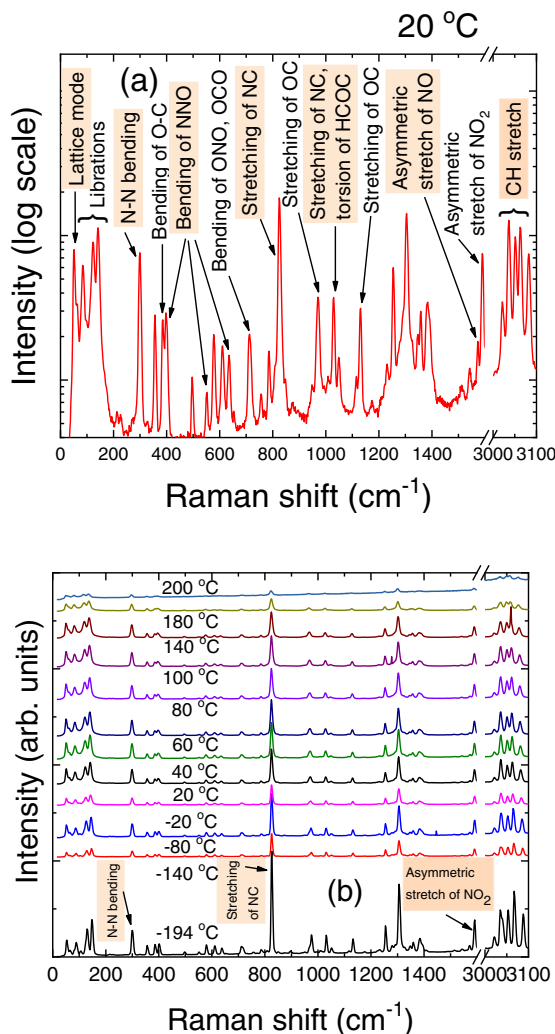


FIG. 5. (a) Ambient Raman spectrum of TEX. The ordinate axis is shown in log scale. (b) Temperature-dependent Raman spectra of TEX at selected temperatures.

modes. This is clear evidence of a structural reorganization in the material. It must also be remarked that there is a sudden kink or hardening just across the beginning of the transition in the elastic modulus (Fig. 4). We observe the same feature in some of the Raman bands. This kind of sudden inflection of vibrational modes at the onset of a transition is common in glassy systems at the glass transition temperature where viscosity lowers and structural relaxations take place in the material.

Figure 7 shows the XRD patterns for TEX at various temperatures. The ambient phase was confirmed to be triclinic [39]. The reflections slightly shift to lower Bragg angles with increasing temperature. Though the patterns do not seem to exhibit any drastic change with temperature, appearance of additional weak reflections (indicated by arrows) is accompanied by softening of Brillouin and Raman modes across the same temperature range, as discussed above. Appearance/disappearance of bands or sudden change of vibrational mode frequencies across a critical thermodynamic parameter (pressure or temperature) observed in Raman spectra is a usual indication of structural reconstruction (a phase transition)

accompanied by change in crystallographic symmetry [41], while sometimes we observe a continuous distortion within the limits of stability of the same phase with variation of pressure or temperature. However, some transitions have been reported [42] to be associated with changes in the electronic states and coordination environment around the atoms, with no change in the crystallographic space group or occupied Wyckoff positions. Such transitions are called isostructural phase transitions. The diffraction intensity (Fig. 7) is shown on a logarithmic scale for the sake of clear visibility of the emerging peaks. The peaks become visible $\sim 50^\circ\text{C}$ and even at 150°C , which is well above the transition; their intensities are significantly smaller than the main peaks. This observation indicates that the high-temperature phase may be isostructural to the low-temperature phase since the Raman modes are similar with very slight change in frequencies. This can then be an isostructural phase transition driven by the phonon softening mechanism, and the slight softening indicates the displacive nature of the transition. A single thermal expansion coefficient of $17.4 \times 10^{-5} \text{K}^{-1}$ for TEX could be determined in our earlier study [39], which suggests similarities in symmetry and unaltered coordination environments around the atoms across the transition [42]. Formation of the new temperature-induced phase takes place over a wide range of temperatures driven by nucleation and growth of the new self-similar phase in the matrix of the room-temperature phase. This is indicative of a conformational change in TEX which does not vary the crystal symmetry. We observed a similar transition in TEX at 2 GPa, where coexistence of exo-exo and exo-endo conformations of molecules were found [4].

A closer look at the Raman mode behavior with temperature shows that the lattice modes and librations soften throughout the temperature range [Fig. 6(a)]. The libration modes exhibit a greater rate of softening with temperature. The bending modes [Figs. 6(b) and 6(c)] exhibit insignificant change of slope before the elastic anomaly. A few bands such as bending of CNC (356 cm^{-1}), in-plane bending of NNO (552 cm^{-1}), bending of NCO (610 cm^{-1}), in-plane bending of NNO (635 cm^{-1}), and in-plane bending of ONO and OCO (712 cm^{-1}) exhibit slight hardening before and after the temperature range of anomaly. The symmetric stretching modes [Fig. 6(d)] depict slight softening throughout the temperature range. However, the OC-stretching vibration at 971 cm^{-1} initially softens and then slightly hardens after 80°C . The asymmetric stretching modes at 1574 cm^{-1} (asymmetric stretch of NO) and 1590 cm^{-1} (asymmetric stretch of NO_2) exhibit hardening in the temperature range $< 20^\circ\text{C}$. However, these modes soften after the onset of the anomalous range. It has been previously shown that, with the increase of pressure, the asymmetric stretch of NO at 1574 cm^{-1} changes from soft to hard behavior $> 3.5 \text{ GPa}$ due to conformational changes in the molecular structure [4]. The presently observed variation with temperature suggests that the intermolecular H bonding (H ... O-N) weakens and elongates with temperature which leads to contraction and hardening of the NO bonds. This expansion of intermolecular hydrogen bonds may result in distortions of the intramolecular geometry of the molecules via change in bond lengths, bond angles, or rotation of molecular fragments. Since the various conformers of TEX are based on the orientation of the NO_2 groups with respect

TABLE II. Raman mode assignments for TEX crystal at ambient temperature.

Raman mode (cm ⁻¹)	Assignment
51 (s)	Lattice mode
63 (w)	Lattice mode
84 (s)	Libration of molecule
123 (s)	Libration of NO ₂
141 (s)	Libration of cage
300 (s)	Out-of-plane bending of N-N; torsion of NCCN
356 (s)	Bending of CNC; torsion of COCO
385 (s)	Stretching and out-of-plane bending of OC; in-plane bending of NNO
398 (s)	In-plane bending of NNO and out-of-plane bending of NCOC
496 (s)	In plane bending of NNO; bending of COC
552 (s)	In-plane bending of NNO
578 (s)	Stretching of NC; stretching of NN
610 (s)	Bending of NCO
635 (s)	In-plane bending of NNO
712 (s)	In-plane bending of ONO; in-plane bending of OCO
785 (s)	In-plane bending of ONO; bending of CNC
825 (s)	Stretching of NC and OC; in-plane bending of COC and ONO
971 (s)	Stretching of OC
1029 (s)	Stretching of NC; torsion of HCOC
1130 (s)	Stretching of OC
1254 (s)	Stretching of NO ₂ ; bending of HCO; torsion of HCOC
1288 (w)	Stretching of NO ₂ , in-plane bending of HCO; torsion of HCOC
1304 (s)	Out of plane bending of HCO; torsion of HCOC
1357 (w)	In-plane bending of HCO
1574 (s)	Asymmetric stretching of NO
1590 (s)	Asymmetric stretching of NO ₂
3021 (s)	CH asymmetric stretching in 5-membered ring
3037 (s)	CH symmetric stretching in 5-membered ring
3051 (s)	CH stretching
3063 (s)	CH asymmetric stretching in 6-membered ring
3082 (s)	CH symmetric stretching in 6-membered ring

to the six-membered cage of the isowurtzitane structure, the anomalous hardening of the modes with temperature $< 20^\circ\text{C}$ switching over to softening indicates a release of stiffness from the NO bond owing to a change of conformation, which begins to show normal softening $> 80^\circ\text{C}$. The behavior of these two asymmetric stretching modes indicates a conformation change at the anomalous range like that observed in our pressure-dependent study [4].

The CH stretching modes [Fig. 6(f)] depict a larger rate of softening like the libration modes. Interestingly, we observe a CH mode splitting at a lower temperature $< -150^\circ\text{C}$, like the splitting of CH symmetric stretch observed at 2 GPa in our previous work [4]. The pressure-dependent splitting of CH stretching is reminiscent of the splitting of modes observed in the secondary explosive with a similar structure CL-20 [43]. This splitting has been assigned to a conformational change from C_2 to C_1 molecular symmetry of $\varepsilon \rightarrow \gamma$ CL-20 [43]. It is possible that a similar conformational change is occurring at lower temperatures also as observed at 2 GPa in TEX crystal. Furthermore, this is the same temperature where we observe an inflation in the elastic modulus (Fig. 4). As temperature is increased, the elastic modulus increases. This is accompanied by a merging of CH modes. This implies strengthening of hydrogen bonds in the CH groups and a closer packing of molecules to average out the CH force constants. Such

slight rearrangement of atoms causes only a deformation or a change in conformation without causing a change in the space group. However, since no other Raman mode exhibits changes $\sim -150^\circ\text{C}$, it is probable that such a splitting in other modes is not observed due to limitation in spectral resolution in these experiments.

A detailed analysis of all important Raman modes of TEX clearly depicts their frequency reduction across the elastic anomaly ($20\text{--}80^\circ\text{C}$), as observed for the longitudinal elastic modulus, except for the bending modes and stretching (971 cm^{-1}) mode. This implies that the in-plane bending of NNO, ONO, and OCO stiffen along with the OC stretching vibration when the temperature rises $> 80^\circ\text{C}$. This hardening associated with these bonds may thus indicate that a fraction of the previous exo-exo conformer still exists, while all other modes soften, indicating a conformational change to exo-endo and aiding the increasing compressibility. It was demonstrated by Zeng *et al.* [11] from their density of states calculations that N-NO₂ is the most chemically active part of the molecule, while ether oxygen forms the second most active part. These points are thus more prone to breakdown from impact and thermal stimuli and hence exhibit changes in phonon behavior.

We have shown above from our elastic constants calculation that TEX possesses high bulk modulus which may contribute to its low sensitivity. However, our

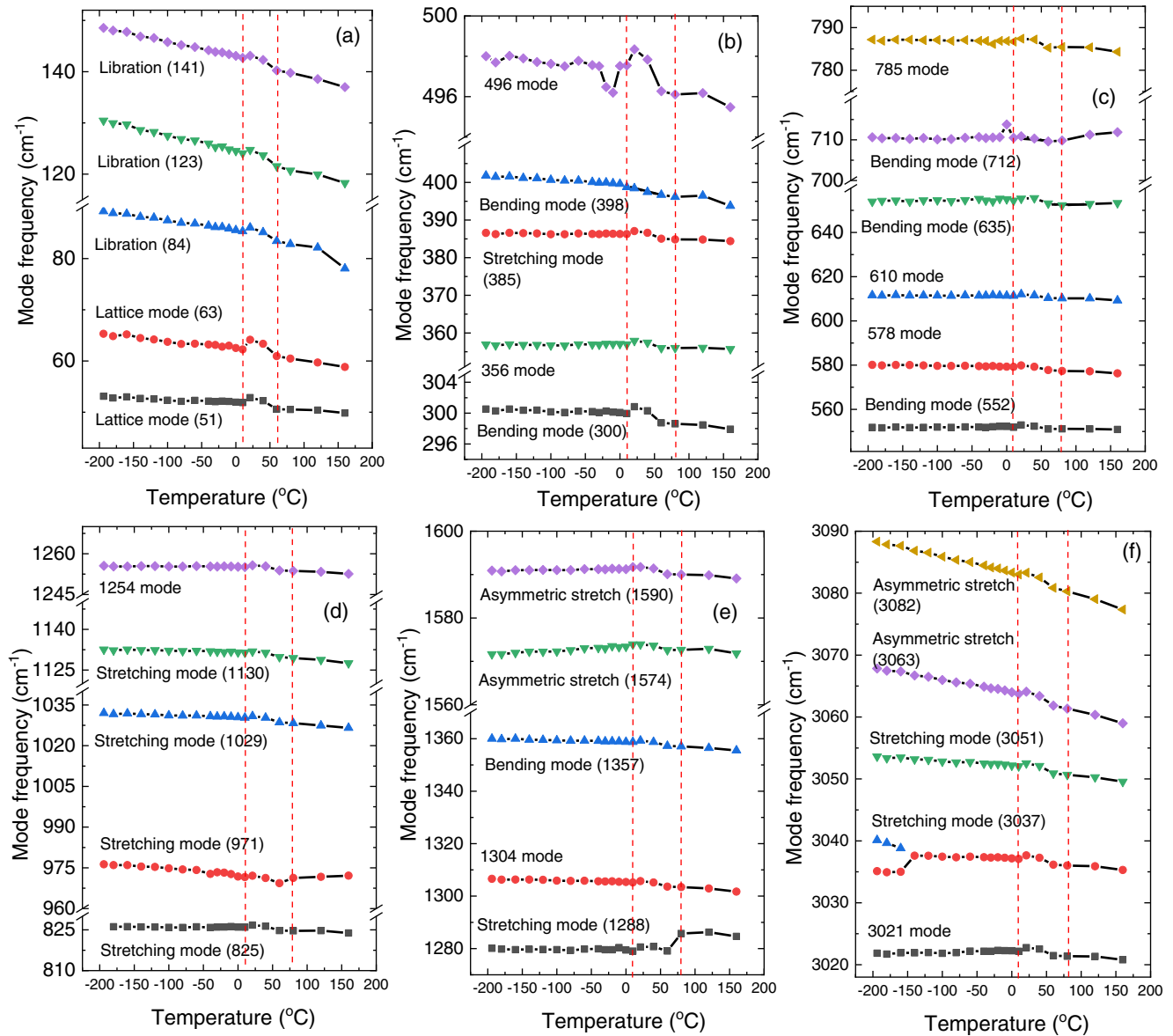


FIG. 6. (a)–(f) Temperature dependence of the Raman mode frequencies of the important bands of TEX crystal. The modes are named according to their position at ambient, as described in Table II. The red vertical dashed lines depict a region with steeper slope of frequency, the temperature range matching the elastic anomaly.

temperature-dependent study of elastic modulus and Raman modes clearly demonstrates an inflation of values around room temperature and thereafter a sudden decrease. This increase in compressibility just above room temperature may result in increased sensitivity of the explosive material. It is a matter of concern that the temperature range of increased compressibility is just above room temperature, and a slight increase in storage temperature or heat generated during handling may spike up the sensitivity and cause accidental damage. Therefore, studies of sensitivity measurements in this temperature range deserve urgent research attention.

IV. CONCLUSIONS

Brillouin and Raman spectra of TEX were recorded as a function of temperature up to 180 °C, close to its m.p.

Each Brillouin spectrum revealed one LA and one TA mode. Both Brillouin and Raman spectra were analyzed for mode frequencies and widths by curve fitting. Ambient values of experimental shear (G) and bulk (K) moduli of TEX are obtained as $G = 5.6$ GPa and $K = 17.7$ GPa. The known lower sensitivity of TEX compared with similar caged secondary explosives is reckoned as due to its inherently high bulk modulus. Here, T variation of acoustic modes revealed an initial monotonic reduction in LA mode frequency and an anomalous dip at ~ 20 °C. Since the acoustic phonons are of long wavelength, any sudden change in their behavior implies a change in long-range intermolecular force constants. In this paper, we report direct experimental evidence of rapid, anomalous reduction in elastic constant of TEX by ~ 5 GPa from 20 to 80 °C, much before its sublimation point (>240 °C). This implies an increase in compressibility and

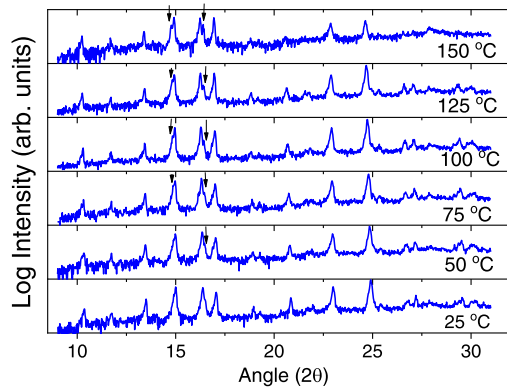


FIG. 7. X-ray diffraction patterns of TEX at various temperatures. The y axis is presented in logarithmic scale. The arrows indicate emergence of new reflections.

hence sensitivity. Though there are no phase transitions in this temperature span, all Raman bands exhibit anomalous behavior around this temperature. We observe two distinct behaviors: (1) a few modes that exhibited hardening behavior below the anomaly continue to blueshift after 80 °C, while (2) some modes hardening <20 °C soften >80 °C. This hardening switching over to softening above the elastic anomalous range indicates a release of stiffness manifesting from a con-

formational change to exo-endo and aiding the increasing compressibility. Emergence of new diffraction peaks ~ 50 °C and even observed at 150 °C, which is well above the elastic anomaly, suggests that the material at high temperature may be isostructural to that at low temperature. Therefore, from a multilength scale analysis using the techniques of Brillouin and Raman spectroscopy, we probed the TEX structure in the bulk and atomic scale. The insights from a combination of these techniques helped investigate the elastic anomaly that starts just above room temperature. In this paper, we establish that the high bulk modulus value of TEX contributes to its lower sensitivity. However, a rapid reduction in elastic modulus accompanied by anomalous behavior of Raman modes may result in increased sensitivity of the explosive material just above room temperature. The anomalous behavior of the in-plane bending of ONO and OCO (712 cm^{-1}) and the OC stretching vibration (971 cm^{-1}) modes above the elastic anomaly may be explored further to understand the relation between sensitivity and stiffness constants. Additional studies need to be conducted to obtain the total elastic tensor of TEX experimentally.

ACKNOWLEDGMENTS

We sincerely thank Dr. Gurpreet Kaur for useful discussions and support in computation. We also thank Dr. N. V. Chandrashekar and Dr. S. Raju for encouragement.

- [1] D. M. Badgular, M. B. Talawar, S. N. Asthana, and P. P. Mahulikar, *J. Hazard. Mater.* **151**, 289 (2008).
- [2] S. Zeman and M. Jungová, *Propellants Explos. Pyrotech.* **41**, 426 (2016).
- [3] P. Politzer and J. S. Murray, *Propellants Explos. Pyrotech.* **41**, 414 (2016).
- [4] R. Rajan, T. R. Ravindran, V. Venkatesan, V. Srihari, K. K. Pandey, S. Chandra, K. K. Mishra, and A. A. Vargeese, *J. Phys. Chem. A* **122**, 6236 (2018).
- [5] T. R. Ravindran, R. Rajan, and V. Venkatesan, *J. Phys. Chem. C* **123**, 29067 (2019).
- [6] D. E. Hooks, K. J. Ramos, C. A. Bolme, and M. J. Cawkwell, *Propellants Explos. Pyrotech.* **40**, 333 (2015).
- [7] J. J. Haycraft, L. L. Stevens, and C. J. Eckhardt, *J. Chem. Phys.* **124**, 024712 (2006).
- [8] S. D. McGrane and A. P. Shreve, *J. Chem. Phys.* **119**, 5834 (2003).
- [9] M. B. Deshmukh, A. U. Borse, P. P. Mahulikar, and D. S. Dalal, *Org. Process Res. Dev.* **20**, 1363 (2016).
- [10] J. K. Nair, M. B. Talwar, R. S. Palaiah, T. Mukundan, and H. Singh, *Def. Sci. J.* **52**, 157 (2002).
- [11] X. L. Zeng, X. H. Ju, and H. X. Gao, *Adv. Mater. Res.* **554–556**, 1618 (2012).
- [12] K. Gańczyk, A. Zygmunt, and T. Gołofit, *J. Therm. Anal. Calorim.* **125**, 967 (2016).
- [13] L.-B. Xiao, F.-Q. Zhao, Y. Luo, H.-X. Gao, N. Li, Z.-H. Meng, and R.-Z. Hu, *J. Therm. Anal. Calorim.* **121**, 839 (2015).
- [14] T. M. Klapötke, K. Karaghiosoff, A. Michailovski, and G. Holl, *Acta Cryst. C* **58**, o580 (2002).
- [15] V. T. Ramakrishnan, M. Vedachalam, and J. H. Boyer, *Heterocycles* **31**, 3 (1990).
- [16] E.-C. Koch, *Propellants Explos. Pyrotech.* **40**, 374 (2015).
- [17] J. J. Haycraft, *J. Chem. Phys.* **131**, 214501 (2009).
- [18] L. L. Stevens and C. J. Eckhardt, *J. Chem. Phys.* **122**, 174701 (2005).
- [19] T. D. Sewell, R. Menikoff, D. Bedrov, and G. D. Smith, *J. Chem. Phys.* **119**, 7417 (2003).
- [20] X.-J. Xu, H.-M. Xiao, J.-J. Xiao, W. Zhu, H. Huang, and J.-S. Li, *J. Phys. Chem. B* **110**, 7203 (2006).
- [21] G. Zhang, S. Jin, L. Li, Y. Li, D. Wang, W. Li, T. Zhang, and Q. Shu, *J. Therm. Anal. Calorim.* **126**, 467 (2016).
- [22] D. Xiang and W. Zhu, *RSC Adv.* **7**, 8347 (2017).
- [23] Z. Liu, Q. Wu, W. Zhu, and H. Xiao, *Can. J. Chem.* **92**, 616 (2014).
- [24] M. J. Frisch, G. W. Trucks, H. B. Schlegel, G. E. Scuseria, M. A. Robb, J. R. Cheeseman, G. Scalmani, V. Barone, B. Mennucci, G. A. Petersson *et al.*, GAUSSIAN 09 (Gaussian, Inc., Wallingford, CT, 2009).
- [25] P. J. Stephens, F. J. Devlin, C. F. Chabalowski, and M. J. Frisch, *J. Phys. Chem.* **98**, 11623 (1994).
- [26] M. D. Hanwell, D. E. Curtis, D. C. Lonie, T. Vandermeersch, E. Zurek, and G. R. Hutchison, *J. Cheminformatics* **4**, 17 (2012).
- [27] M. D. Segall, P. J. D. Lindan, M. J. Probert, C. J. Pickard, P. J. Hasnip, S. J. Clark, and M. C. Payne, *J. Phys.: Condens. Matter* **14**, 2717 (2002).
- [28] T. H. Fischer and J. Almlof, *J. Phys. Chem.* **96**, 9768 (1992).
- [29] D. M. Ceperley and B. J. Alder, *Phys. Rev. Lett.* **45**, 566 (1980).

- [30] J. P. Perdew and A. Zunger, *Phys. Rev. B* **23**, 5048 (1981).
- [31] H. J. Monkhorst and J. D. Pack, *Phys. Rev. B* **13**, 5188 (1976).
- [32] S. A. Thomas, R. S. Hixson, M. C. Hawkins, and O. T. Strand, *Int. J. Impact Eng.* **139**, 103506 (2020).
- [33] H. M. Ledbetter, *J. Phys. D Appl. Phys.* **13**, 1879 (1980).
- [34] J. G. Berryman, *J. Comput. Phys.* **271**, 379 (2014).
- [35] C. M. Kube and M. de Jong, *J. Appl. Phys.* **120**, 165105 (2016).
- [36] R. Hill, *Proc. Phys. Soc. A* **65**, 349 (1952).
- [37] H. Yao, L. Ouyang, and W.-Y. Ching, *J. Am. Ceram. Soc.* **90**, 3194 (2007).
- [38] S. Chakraborty, A. K. Arora, V. Sivasubramanian, P. S. R. Krishna, and R. Venkata Krishnan, *J. Phys.: Condens. Matter* **24**, 505401 (2012).
- [39] R. Rajan, T. R. Ravindran, R. Raja Madhavan, R. Asuvathraman, S. Chandra, V. Venkatesan, and A. A. Vargeese, *J. Mol. Struct.* **1195**, 859 (2019).
- [40] J. A. Mandarino, *Canad. Mineral.* **17**, 71 (1979).
- [41] E. V. Boldyreva, *Cryst. Eng.* **6**, 235 (2003).
- [42] D. Saha, R. Ranjan, D. Swain, C. Narayana, and T. N. Guru Row, *Dalton Trans.* **42**, 7672 (2013).
- [43] J. A. Ciezak, T. A. Jenkins, and Z. Liu, *Propellants Explos. Pyrotech.* **32**, 472 (2007).